Fundamental Investigation on Electrostatic Ink Jet Phenomena in Pin-to-Plate Discharge System

Hiroyuki Kawamoto†♦, Shinjiro Umezu and Ryuta Koizumi
Department of Mechanical Engineering, Waseda University, Shinjuku, Tokyo, JAPAN

A fundamental investigation was conducted on electrostatic ink jet phenomena. High voltage was applied between an insulative capillary tube filled with ion conductive water and a metal plate electrode. A large water drop was formed and dropped from the tube at the dark discharge under conditions of appropriate voltage application and water level. The diameter of the drop was about one millimeter. At the beginning of corona discharge, however, a Taylor cone of water was formed at the tip of the tube and the tip of the cone was broken to form a very small droplet that was dispersed like mist at wide angle due to the Coulomb repulsive force of charged mist. When the applied voltage was further increased, water droplet was formed periodically. Application of adjusted pulse voltage can form a droplet of which formation is synchronized with the pulse. The diameter of the droplet depended on the applied voltage and the tube diameter. It was less than a Rayleigh's limit and agreed fairly well with a Vonnegut's limit. Preliminary printing on a paper was also demonstrated. This phenomenon is expected to be utilized for a new ink jet print head.

Journal of Imaging Science and Technology 49: 19–27 (2005)

Introduction

Electrostatics of a pin-to-plate gas discharge system have been widely investigated mainly in the field of the high voltage engineering. In addition to the electrical aspects, the authors have been studying kinetics of the system,[1–4] because it is an important basis for some issues in electrophotography, such as dynamics of a pin charger,[2] a cleanerless brush charger, and a "bead carry-out" phenomenon with a magnetic brush development subsystem.[5–7] Another interest is an ink jet system. It is well known that an electrostatic ink jet phenomenon is observed[8–12] when a tube filled with ink is used for the pin electrode. Although drop-on-demand (DOD) ink jet printing is currently dominated by thermal and piezoelectric technologies, another new DOD print head technology is expected to be realized, if the formation of ink droplets can be controlled by the application of the electrostatic field to the liquid. It is expected to be applied not only for ink jet printing systems but also for biological and analytical chemistry,[13] electrospray, and for film formation for microelectronic devices.

Electrospraying and its application have been investigated by many investigators since the first work by Rayleigh[14] on the stability of a charged liquid drop. He deduced that there is a limit to the charge that can be sustained by the drop, above which it becomes unstable and disrupts. This limit is known as the Rayleigh limit. Although a number of workers have investigated the effect of an electrostatic field at a liquid surface since then, works of Vonnegut and Neubauer[15] in 1952 and Taylor[16] in 1964 are especially interesting and important. Vonnegut and Neubauer established the relationship between the charge-to-volume ratio of a droplet applying the energy minimization principle. This Vonnegut limit is equal to half the Rayleigh limit. Taylor showed both theoretically and experimentally that an electrostatically stressed liquid surface can be distorted into a stable conical shape called a Taylor cone, of which the semi-vertex angle is 49.3°.

In any published study, however, nothing appears to have been reported on the relationship between the electrospraying phenomena and the mode of gas discharge, in spite of the fact that kinetics of dark discharge are quite different to those of corona discharge in a pin-to-plate gas discharge system. That is, at low applied voltage, less than corona onset, a Coulomb attractive force is applied to the pin electrode. However, when the corona discharge takes place at a voltage higher than the threshold, substantial ionic wind flows from the pin electrode to the plate electrode. This causes a repulsive force to the pin electrode.

Although many studies have also been published on electrostatic ink jet and some interesting technologies have been introduced, they have been performed mainly for industrial application,[10,11] and the basic research is not enough, especially concerning the relationship be-

Original manuscript received January 12, 2004

♦ IS&T Fellow

†Corresponding Author: H. Kawamoto, kawa@waseda.jp

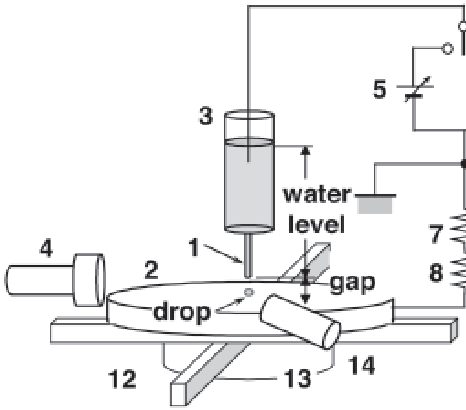

Figure 1. Experimental set-up. (1: water pin electrode, insulative capillary tube filled with ion-conductive water, 2: metal plate electrode, 3: syringe, 4: CCD camera, 5: DC high voltage power supply, 6: high voltage amplifier, 7: shunt resistor, 400 kΩ, 8: resistor: 400 kΩ, 9: function generator, 10: oscilloscope, 11: volt meter, 12: linear motors, x and y directions, 13: mechanical z-stage, 14: stroboscope light).

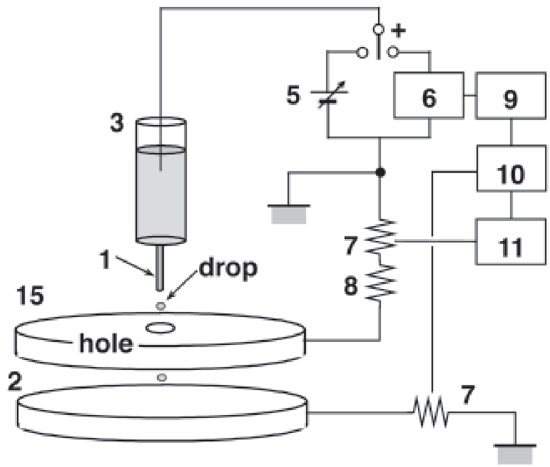

Figure 2. Experimental set-up. (15: metal plate electrode with hole).

tween the ink jet phenomenon and the mode of gas discharge. The purpose of our investigation is to clarify how the formation of the droplet in the electrostatic and corona discharge field is influenced by the mode of discharge, by use of kinetics in the pin-to-plate gas discharge field.

Experimental

An experimental set-up illustrated in Fig. 1 was constructed to investigate characteristics of the formation of water droplets in the electrostatic field. The capillary tube made of silica coated by polyimide (Polymicro Technologies, Phoenix, AZ) was equipped with a bottom of a syringe. Two kinds of tube were used for experiments; one had 50 µm inner and 170 µm outer diameters and another had 100 µm inner and 170 µm outer diameters. Although the preceding researches were conducted with a metal tube,[10–13] we used an insulating tube for simplification of the phenomenon, insofar as the electrostatic force acted only on water. Ion conductive water was poured into the syringe and injected into the insulating tube. This tube with water was mounted perpendicular to a plate electrode made of stainless steel. DC voltage was applied by a DC power supply (Matsusada Precision Inc, Tokyo, HVR-10P) and pulse voltage was generated with a function generator (Iwatsu, Tokyo, SG-4105) and a high voltage amplifier (Matsusada Precision Inc, HEOP-10B2). The voltage was measured by a digital oscilloscope and the current was measured by the voltage drop across a current-shunt resistor. The formation of the droplet was observed with a CCD microscope camera (Keyence, Tokyo, VH-7000). A high-speed microscope camera (Redlake MASD, San Diego, CA, Motion-Meter 1140-0003) was also used with a stroboscope light (Sugawara Laboratories Inc., Kawasaki, Japan, NP-1A) to observe transient formation and separation of droplets. The gap was adjusted by a z-stage and the plate electrode was moved in x and y directions with two linear stages to demonstrate ink jet printing on a paper.

Another modified set-up, shown in Fig. 2, was constructed to measure the charge on an individual droplet. A small hole, 5 mm in diameter, was opened at the center of the plate electrode and another plate electrode was set at the back of the plate parallel to it. In this configuration, corona current flowed solely to the upper plate but the charge of droplet was transferred to the lower plate. Therefore, the charge on the droplet was separated from the corona current, and was measured by integrating the current flowing to the lower plate. We confirmed that no corona current flowed to the lower plate electrode with a metal pin electrode.

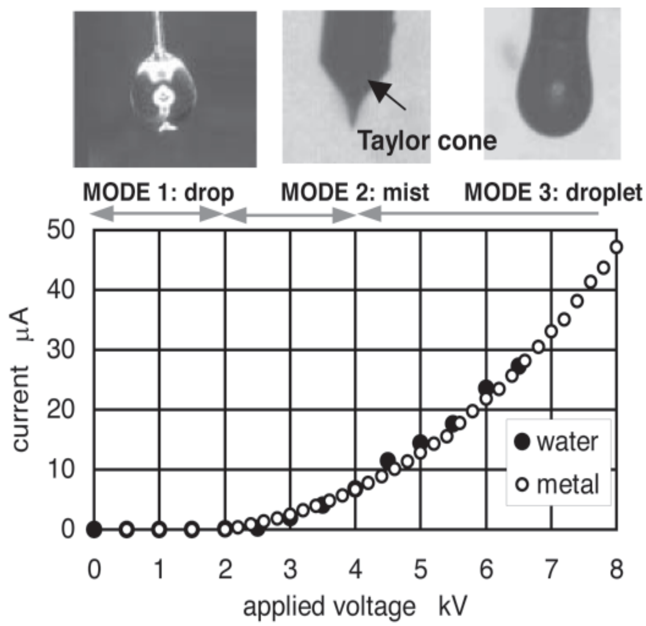

Figure 3. V-I curves in pin-to-plate electrode system. (100 µm inner tube diameter, 100 µm metal pin diameter, 3 mm air gap).

Fundamental Characteristics

In the first place, the current-voltage characteristics of the water pin electrode were measured and compared with those of the metal pin electrode of the same diameter as the inner diameter of the insulating tube. The results are shown in Fig. 3. In case of the water pin

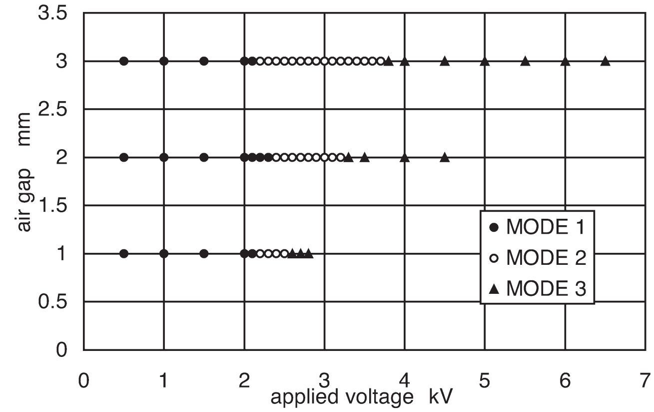

Figure 4. Relationship between applied voltage and air gap versus mode of drop formation (1). (100 µm inner tube diameter).

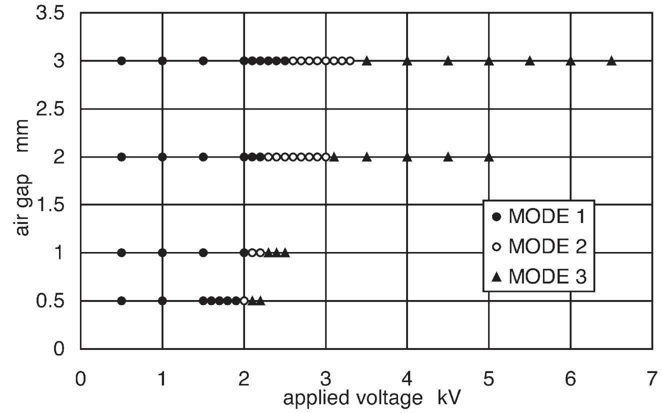

Figure 5. Relationship between applied voltage and air gap versus mode of drop formation (2). (75 µm inner tube diameter).

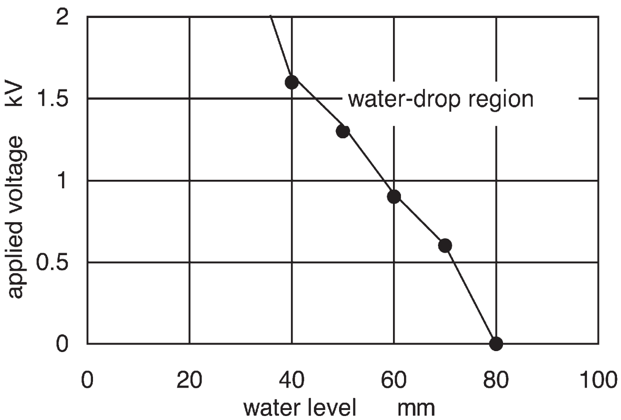

Figure 6. Critical water level and voltage of water dropping in dark discharge regime. (3 mm air gap, 100 µm inner tube diameter).

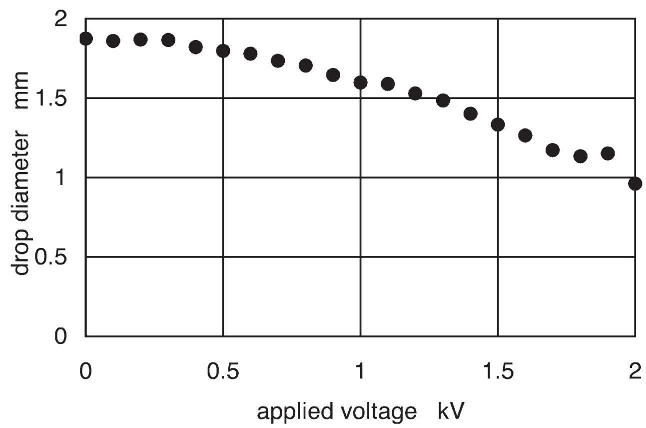

Figure 7. Applied voltage versus critical diameter of drop in dark discharge regime. (3 mm air gap, 90 mm water level, 100 µm inner tube diameter).

electrode, although a pulse current was superposed on the corona current, corresponding to the separation of the droplet, as described below, a stable corona current was measured and plotted in the figure. Corona current of the water electrode agreed well with that of the metal pin electrode and fundamental characteristics of the discharge were common. That is, no current flowed in the dark discharge regime, however, when the applied voltage reached a threshold (about 2 kV), corona discharge took place, and the corona current in the order of microA flowed.

As added in Fig. 3 the formation of the droplet was classified into the following three modes corresponding to the discharge modes.[9]

MODE 1: In the dark discharge regime, 0 ~ 2 kV, a drop was formed at the tip of the tube. This became gradually larger and finally separated. The diameter of the drop was several times larger than that of the tube diameter and the drop period was long, more than a second.

MODE 2: At the beginning of the corona discharge, 2 ~ 4 kV, a Taylor cone was formed at the end of the tube and the tip of the cone periodically separated from the cone to form a very small droplet of the order of several tens of microns in diameter. Droplets dispersed over a wide angle, like a mist.[12] Trajectory of the droplet was unstable and the frequency of the droplet formation was very high, in the order of kHz.

MODE 3: At still higher voltage, the Taylor cone changed to hemispherical and the droplet became relatively large, nearly the same as the tube diameter. The frequency of the droplet formation was 10 ~ 100 Hz.

Figures 4 and 5 show how these three modes were determined by the applied voltage, the air gap, and the inner tube diameter. The voltage range of MODE 2 became wide when the air gap was large.

At the Dark Discharge Regime

Critical Voltage and Water Level of Drop Separation

Figure 6 shows the critical applied voltage and the critical water level, the length between top level of water in the syringe and the lower end of the tube (refer to Fig. 1), when the drop just separated from the tube in the dark discharge regime (MODE 1). It is evident that the drop was formed under conditions of high pressure and high electrostatic field.

Critical Diameter of Drop

Figures 7, 8, and 9 show how the drop diameter at the separation of the drop from the tube was determined by the applied voltage, the air gap, and the water level, respectively. The critical diameter was small under con-

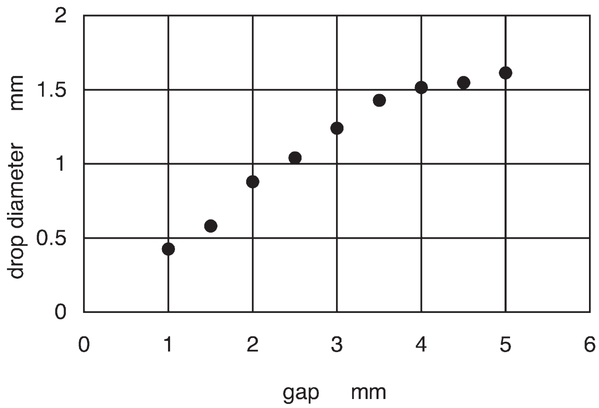

Figure 8. Air gap versus critical drop diameter in dark discharge regime. (90 mm water level, 100 µm inner tube diameter, 1.6 kV applied voltage).

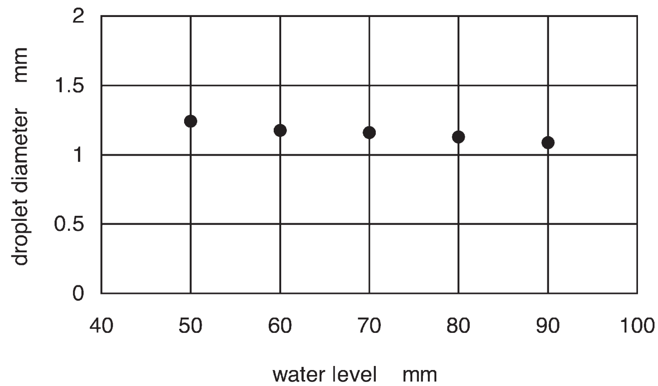

Figure 9. Water level versus critical diameter of drop in dark discharge regime. (3 mm air gap, 100 µm inner tube diameter, 1.6 kV applied voltage).

ditions of high voltage and small gap. This means that the electrostatic force applied to the drop forced the drop to separate from the tip of the tube before it grew to full size.

Balance of Forces Applied to Drop

In the dark discharge regime, forces applied to the drop at the tip of the tube are the electrostatic Coulomb force F_e, force due to surface tension F_s, force due to water pressure F_p, and weight of the drop mg. It is assumed that the critical diameter was determined as a static balance of these forces. Hoop tension due to charge on the drop was neglected, because no measurable charge existed in the drop formed in the dark discharge regime. Thus,

$$F_e = F_s - F_p - mg = 2\pi r_o \gamma - \pi r_i^2 \rho g h - \frac{4}{3}\pi r_d^3 \rho g, \quad (1)$$

where r_o is the outer radius of the tube, 75 µm, γ is surface tension of water measured by the ring method, 63 N/m, r_i is the inner radius of the tube, 50 µm, ρ is the density of water, h is the water level, and g designates the gravitational constant. To confirm this hypothesis the electrostatic force, F_e, was derived by substitution of the measured critical conditions into Eq. (1), and, it was compared to the force separately measured with the metal pin electrode. Experimental methods to measure the force applied to the meal electrode have been reported in Ref. 1. Here, the diameter of the metal pin electrode, 1.2 mm, was adjusted to be approximately the same as that of the drop. It is clearly recognized from the result shown in Fig. 10 that the force derived from the critical drop agreed well with that of the metal pin electrode, and they were proportional to the square of the applied voltage. From this experimental evidence it is simply concluded that the critical diameter was determined as a static balance of the Coulomb force, the surface tension, the water pressure, and gravity. However, the diameter was too large and a period of the drop formation too long for ink jet application.

At the Beginning of Corona Discharge

Mechanism of Mist Formation

At the beginning of the corona discharge, a Taylor cone was formed at the end of the tube, and the tip of the Taylor cone separated periodically from the cone to form a very small droplet (MODE 2). Droplets dispersed like

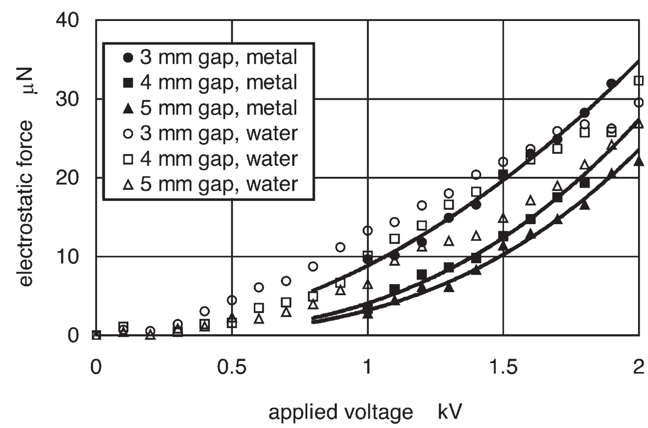

Figure 10. Electrostatic Coulomb force applied to water drop and metal electrode in dark discharge regime. Solid lines are least-square fitted quadratic curves of the metal electrode. (1.2 mm metal pin diameter, 100 µm inner tube diameter in case of water electrode).

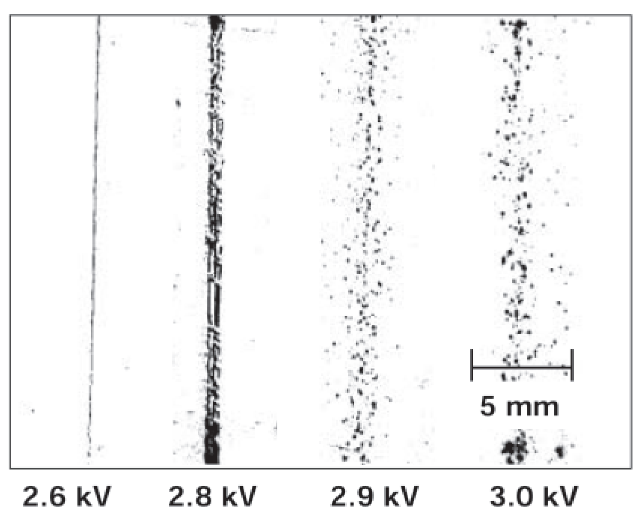

Figure 11. Traces of mist at the beginning of corona discharge. (3 mm air gap, 70 mm water level, 100 µm inner tube diameter, 48 mm/s linear motor speed).

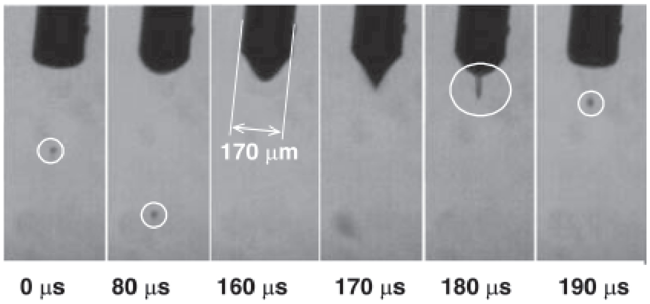

Figure 12. Formation of Taylor cone and mist at the very beginning of corona discharge. (3 mm air gap, 70 mm water level, 100 µm tube diameter, 2.5 kV applied voltage).

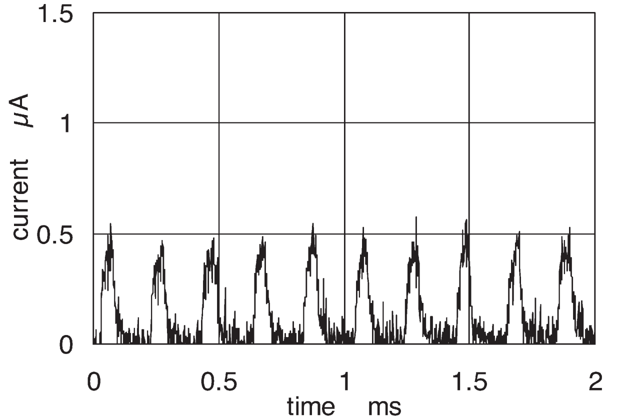

Figure 13. Current corresponding to formation of Taylor cone and mist at the very beginning of corona discharge. (3 mm air gap, 70 mm water level, 100 µm diameter, 2.5 kV applied voltage).

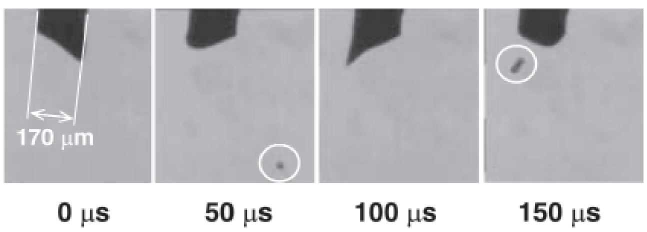

Figure 14. Formation of Taylor cone and droplet at the beginning of corona discharge. (3 mm air gap, 70 mm water level, 100 µm inner tube diameter, 2.6 kV applied voltage).

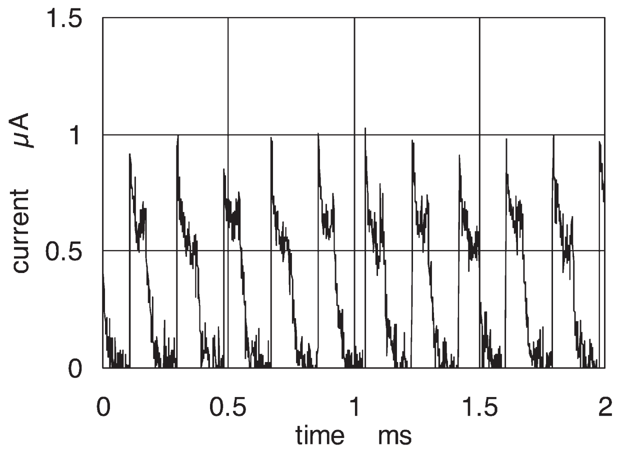

Figure 15. Current corresponding to formation of Taylor cone and mist at the beginning of corona discharge. (3 mm air gap, 70 mm water level, 100 µm inner tube diameter, 2.6 kV applied voltage).

mist over a wide angle, depending on the applied voltage. Figure 11 shows traces of ink mist on a paper. Here, the paper was set on the plate electrode and the plate electrode with paper was linearly driven in y-direction at constant speed to visualize the mist dispersion. It is clearly seen that droplets dispersed widely, even at relatively high applied voltage.

Transient phenomena during droplet formation were observed by the stroboscope light and the high speed camera in order to investigate the mechanism of mist formation. Figure 12 shows photographs on the formation of the Taylor cone and droplets at the very beginning of the corona discharge. The Taylor cone was formed as a balance between the surface tension and the electrostatic force, because the electrostatic field was concentrated at the tip of the water electrode under these conditions. It is assumed that dispersion of the force balance causes the separation of the droplet at the tip of the Taylor cone. It was confirmed that a pulse current was superimposed on the corona current corresponding to the separation of the droplet as shown in Fig. 13, because the frequency of the pulse current was coincided with that of the droplet separation.

If the applied voltage was slightly increased, the shape of Taylor cone became unstable, and the droplet did not drop right under the tube but dispersed as shown in Fig. 14. A Coulomb repulsive force seems to cause this instability, and charged droplets of common polarity spread along the electrostatic flux line. Because ionic wind is very week in this regime, no substantial bundling force was applied to the mist. A separate experiment and numerical calculation indicated that the speed of the ionic wind at the center of the gap was essentially zero m/s under these conditions.[17] Fluctuation of current due to the streamer corona is another possible reason for this instability, but details are not clear so far. The pulse current was increased corresponding to the increase of the applied voltage, but the pulse frequency, i.e., the frequency of the droplet formation, was almost the same as at the very beginning of the corona discharge, as shown in Fig. 15.

If the applied voltage was further increased, both the diameter of the droplet and the frequency varied as shown in Fig. 16 and 17. Taylor cone formation was suppressed probably because the reaction force of the ionic wind became large, and the concentration of the electric field at the tip was accordingly relaxed.[1] This is a transition from MODE 2 to MODE 3. It was confirmed that a relatively large droplet caused the large pulse current, and the pulse current corresponding to the small droplets was small.

Diameter and Charge of Droplet

Figure 18 shows the diameter of the droplet as a function of the applied voltage and the air gap. It was much smaller than that of MODE 1, because only the tip of Taylor cone formed a droplet at MODE 2. The diameter became large at high voltage. There are two possible

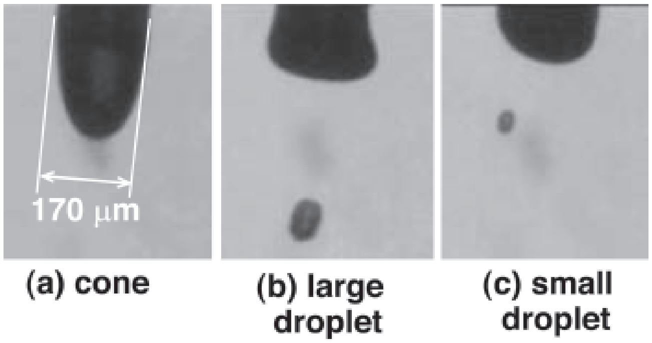

Figure 16. Formation of Taylor cone and droplet at the middle stage of corona discharge. (3 mm air gap, 70 mm water level, 100 μm inner tube diameter, 2.9 kV applied voltage).

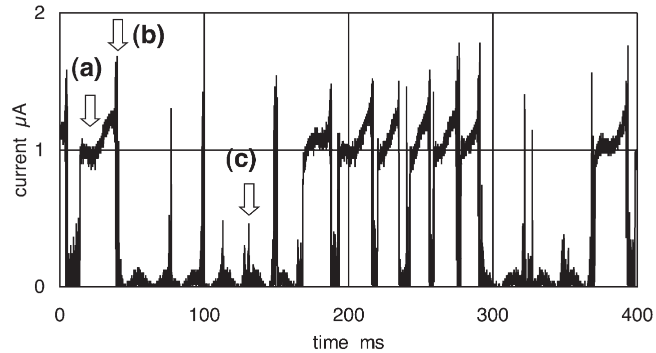

Figure 17. Current corresponding to formation of Taylor cone and mist at the middle stage of corona discharge. (3 mm air gap, 70 mm water level, 100 μm inner tube diameter, 2.9 kV applied voltage).

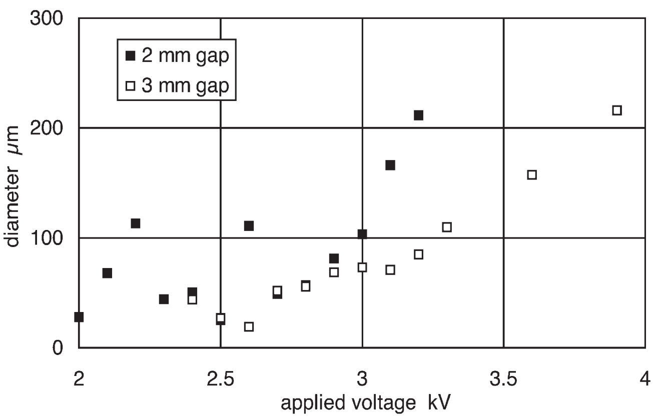

Figure 18. Diameter of droplet at the beginning of corona discharge. (70 mm water level, 100 μm inner tube diameter).

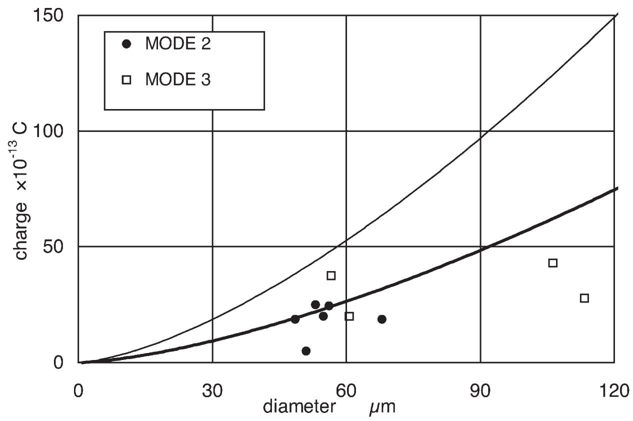

Figure 19. Relationship between the critical droplet diameter and charge. (3 mm air gap, 70 mm water level, 100 μm inner tube diameter).

reasons of this characteristic: one is that the reaction force of the ionic wind prevented the separation of the droplet from the tip of the Taylor cone, and another is relaxation of the electric field, which made the tip of the Taylor cone relatively round. Further investigation is necessary on the mechanism of the droplet formation in the MODE 2 regime, for it is anticipated that MODE 2 may be utilized for a micromist spray and formation of the small droplets.

As qualitatively discussed in the previous section, we assume that the break of the force balance between Coulomb repulsive force and surface tension causes the separation of the droplet at the tip of the Taylor cone. This condition is determined by the following Rayleigh limit.[14,18]

$$Q = 8\pi\sqrt{\varepsilon_0 \gamma R^3} \quad (2)$$

where Q is charge of droplet, ε_0 is the permittivity of free space and R is the radius of the droplet. Another model was established by Vonnegut and Neubauer based on the energy minimization principle.[15] The Vonnegut charge is half the Rayleigh limit. Figure 19 shows Rayleigh's and Vonnegut's limits and the measured relationship between droplet diameter and charge. Measured results were lower than Rayleigh's limit but agreed fairly well with Vonnegut's limit.

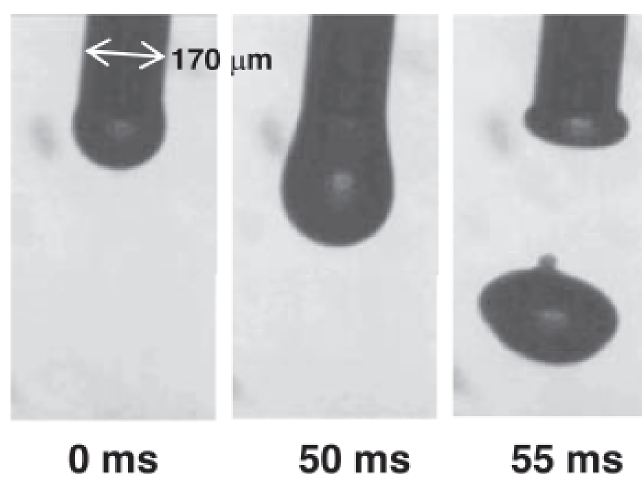

Figure 20. Photograph of droplet formation under conditions of the stable corona discharge. (3 mm air gap, 70 mm water level, 100 μm inner tube diameter, 4.5 kV applied voltage).

At Stable Corona Discharge

At higher voltage, more than 4 kV, Taylor cone formation was suppressed and relatively large droplets were formed as shown in Fig. 20. This is probably because

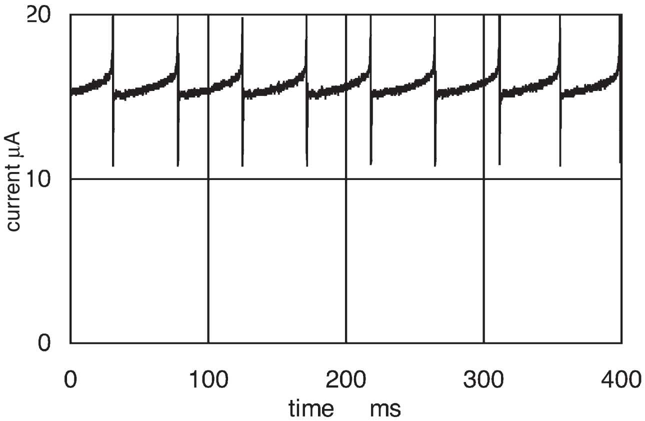

Figure 21. Pulse current corresponding to spraying of water in the stable regime of corona discharge. (3 mm air gap, 70 mm water level, 100 μm inner tube diameter, 4.5 kV applied voltage).

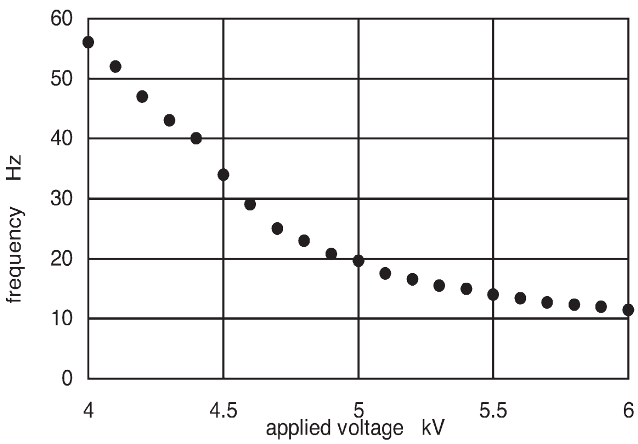

Figure 23. Frequency of current pulse corresponding to water spraying in the stable regime of corona discharge. (3 mm air gap, 90 mm water level, 100 μm inner tube diameter).

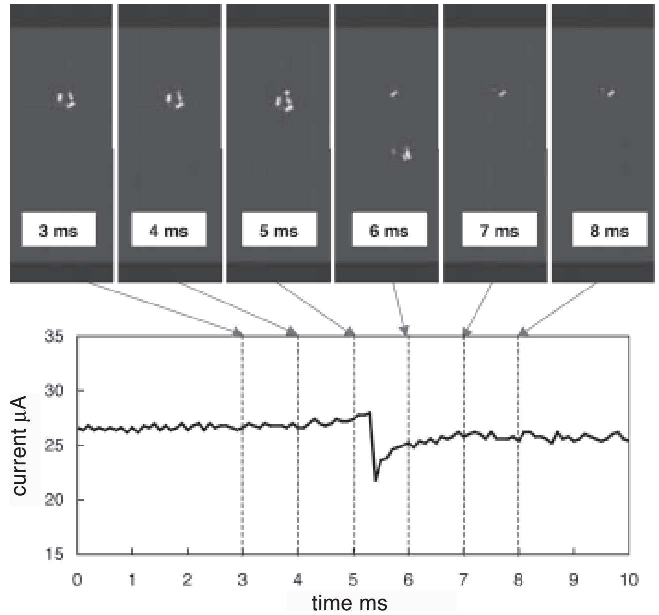

Figure 22. Photographs of dropping of water droplet and corresponding discharge current just at the separation of water droplet. (5 mm air gap, 90 mm water level, 100 μm inner tube diameter, 7 kV applied voltage).

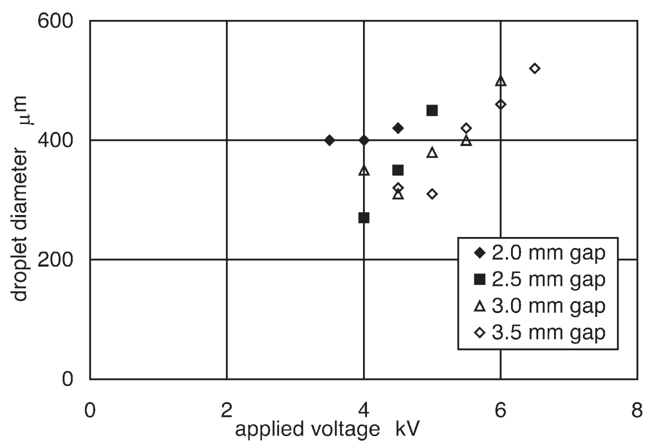

Figure 24. Applied voltage versus droplet diameter in MODE 2 regime. (70 mm water level, 100 μm inner tube diameter, parameter: air gap).

the reaction force of the ionic wind became large, and the concentration of the electric field was relaxed as discussed in the preceding section. A periodic spike current was observed as shown in Fig. 21, corresponding to periodic formation of droplets. It is assumed that convection of the charged droplet is the cause of the spike current. This is confirmed by a synchronized measurement of current and high speed photography of droplet formation. The result is shown in Fig. 22. It was observed that the current increased slightly due to the growth of the droplet, thus shortening the gap, and then suddenly decreased just when the drop separated from the tube. Because a substantially strong ionic wind was generated in this regime, of the order of several m/s,[17] and it streamed to downward from the tip, the charged droplet was neither broken nor deflected, and the single droplet reached the center of the plate electrode in each cycle. This assumption is supported qualitatively by the experimental fact that water level is depressed on the order of several mm under these conditions, if the plate electrode is replaced with water.[3]

Relationship between applied voltage and frequency of the current pulse is shown in Fig. 23. It seems paradoxical that the droplet formation was less frequent at higher voltage. The reason is probably that the repulsive force of the ionic wind acting on the droplet at the tube tip was high at high voltage, but, on the other hand, the attractive force is constant even at high voltage, because the electrostatic field at the tip is maintained constant during corona discharging.[1]

This hypothesis is supported by the experimental results on droplet size. Measured droplet diameter is shown in Fig. 24. Not only the applied voltage but also the air gap was selected as parameters. First of all, it is evident that the higher the voltage the larger the droplet. Because the repulsive force due to the ionic wind acting on the droplet prevented separation of the droplet from the tip of the tube, the droplet grew large before separation at high voltage. Figure 24 indicates that the droplet volume did not depend on the gap. This evi-

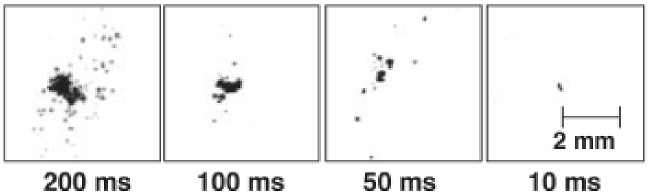

Figure 25. Traces of mist on application of pulse voltage. (3 mm air gap, 70 mm water level, 100 μm inner tube diameter, 3.5 kV-1 Hz applied voltage, pulse width: parameter).

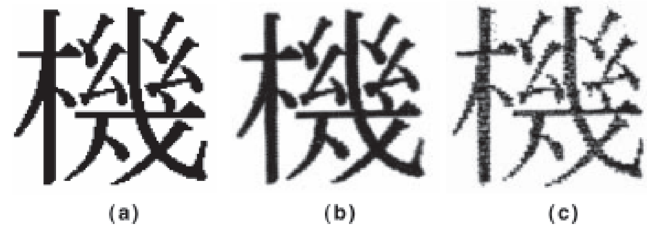

Figure 26. Original (a) and printed samples (b) (c) of Chinese character "Mechanics."
(a) original bit image, 64 × 64 pixel
(b) print sample of MODE 2 droplets: 181 dpi, 100 × 100 dots, 50 μm inner tube diameter, 0.5 mm gap, 1.5 kV applied voltage
(c) print sample of MODE 3 droplets: 50 dpi, 50 × 50 dots, 100 μm inner tube diameter, 3 mm gap, 4.5 kV applied voltage

dence also supports our hypothesis, because the repulsive force rarely depends on the gap.[1]

Demonstration of Ink Jet Printing

For the ink jet printing application, a pulse voltage was applied to control formation of a single droplet. Figure 25 shows traces of mist by application of voltage pulses in the MODE 2 regime. Although droplets dispersed at wide angle with long pulse width, it is possible to control formation of a single droplet by short pulse width voltage application. Printing on paper was demonstrated utilizing this characteristic. A print sample is shown in Fig. 26 (b), application of pulsed voltage, 1.5 kV and 10 ms pulse width, to the pin electrode while a sheet of paper on the plate electrode was linearly driven stepwise in x and y directions by the two linear motors synchronized with the pulse. The speed of motion was 100 ms/step. Ink used for the demonstration was commercially available pigmented black ink for Epson ink jet printers, the paper was not for ink jet printers but for laser printers. Although the present image was preliminary, it is expected to be the basis of a new ink jet system.

We also tried to control droplet formation in the MODE 3 regime for ink jet printing. The pulse width with which the single droplet was formed in one pulse was measured at a fixed frequency. The result is shown in Fig. 27. Critical pulse width depended on the pulse voltage but the frequency was nearly irrelevant. This characteristic was also utilized for the printing as demonstrated and shown in Fig. 26(c). Because the diameter of the droplet in this regime was larger than that at the MODE 2 regime, resolution was poor compared to that of MODE 2. The tube diameter must be smaller to realize higher resolution.

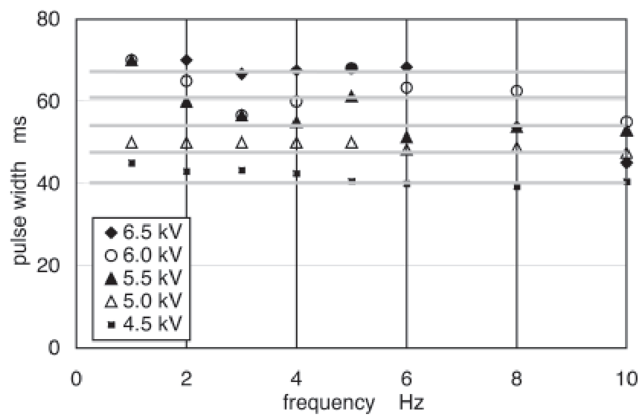

Figure 27. Pulse voltage frequency versus critical pulse width that separates a drop from the tip of the tube. (3 mm air gap, 70 mm water level, 100 μm inner tube diameter, parameter: applied voltage).

Conclusions

We have investigated electrostatic ink jet phenomena in the gas discharge field between an insulative tube filled with ion conductive water and a plate electrode. Principal results of the investigation are as follows.

1. In the dark discharge regime, a relatively large drop is formed at the end of the tube. The diameter of the drop was several times larger than that of the tube diameter and the drop period was long. A critical diameter was determined as a balance of Coulomb force, surface tension, water pressure, and gravity.
2. At the beginning of corona discharge, a Taylor cone of water was formed at the tip of the tube and the tip of the cone broken off to form very small droplets that dispersed like mist over a wide angle due to the Coulomb repulsive force of the charged mist. Droplet diameter was in the order of several tens of microns, and the frequency of droplet formation was very high, on the order of kHz.
3. At the stable stage of corona discharge, the Taylor cone changed to hemispherical and the droplet became relatively large, of the same order of the tube diameter. The frequency of the droplet formation was 10 – 100 Hz.
4. In any case, the diameter of the droplet depended on applied voltage and tube diameter. It was less than the Rayleigh limit but agreed fairly well with the Vonnegut limit.
5. Application of an adjusted voltage pulse can lead to droplet formation synchronized with the pulse. Printing on paper was demonstrated utilizing this characteristic.

Acknowledgment. The authors would like to express their thanks to Kenji Arai, Hodaka Suzuki, and Ryosuke Nakazawa for their help of carrying out experiments. This work is supported by The 21st Century COE Program of Japan Society for Promotion of Science and The Asahi Glass Foundation's Research Grant.

References

1. H. Kawamoto, Statics of pin corona charger in electrophotography, *J. Imaging Sci. Technol.* **45-6,** 556–564 (2001).
2. H. Kawamoto, K. Takasaki, H. Yasuda, and N. Kumagai, Dynamics of pin electrode in pin-to-plate gas discharge system used for ozoneless charger in laser printer, *10th ICPE: The 10th Int. Conf. on Precision Engineering*, The Japan Society for Precision Engineering, Yokohama, Japan, 2001, pp. 694–698.

3. H. Kawamoto, K. Takasaki and H. Yasuda, Dynamics of pin electrode in pin-to-plate discharge system, *IS&T's NIP17: Int. Conf. on Digital Printing Technologies*, IS&T, Springfield, VA, 2001, pp. 682–689.
4. H. Kawamoto, K. Takasaki, H. Yasuda, S. Umezu and K. Arai, Static and dynamic phenomena of pin electrode in pin-to-plate discharge system, *Proc. of the 3rd. IFToMM Int. Micromechanism Symp.*, 2001, pp. 69–74.
5. E. M. Williams, *The Physics and Technology of Xerographic Processes*, Krieger Publishing Co., Malabar, FL, 1993, p. 200.
6. N. Nakayama, H. Kawamoto and M. Nakatsuhara, Electrostatic pull-off of magnetic bead chains in two-component magnetic development system of electrophotography, *Proc. of the 2003 JSME-IIP/ASME-ISPS Joint Conf. on Micromechatronics for Information and Precision Equipment: IIP/ISPS Joint MIPE,* The Japan Society of Mechanical Engineers, Tokyo, Japan, 2003, pp. 323–324.
7. N. Nakayama, Y. Watanabe, Y. Watanabe, and H. Kawamoto, Experimental and numerical study on the bead-carry-out in two-component development process in electrophotography, *IS&T's NIP19: Int. Conf. on Digital Printing Technologies*, IS&T, Springfield, VA, 2003, pp. 69–73.
8. A. Bailey, *Electrostatic Spraying of Liquids*, Research Studies Press, Tounton, Somerset, England, 1988, pp. 60–90.
9. M. Cloupeau and B. Prunet–Foch, Electrohydrodynamic spraying functioning modes: A critical review, *J. Aerosol Soc,* **25,** 1021–1036 (1994).
10. R. Mills, ESIJET™ printing technology, *IS&T's NIP 12: Int. Conf. on Digital Printing Technologies*, IS&T, Springfield, VA, 1996, pp. 262–266.
11. T. Murakami, S. Hirahara, H. Nagato, H. Nakao, and Y. Nomura, High definition ink-jet printing with electrostatic force, *J. Imaging Soc. Japan* **40-1,** 40–47, 2001 (in Japanese).
12. J-D. Moon, J-G. Kim and D-H. Lee, Electrophysicochemical characteristics of a waterpen corona discharge, *IEEE Trans. Industry Applications* **34-6,** 1212–1217 (1998).
13. O. Yogi, T. Kawakami, M. Yamauchi, J. Yong Ye, and M. Ishikawa, On-demand droplet spotter for preparing pico-to femtoliter droplets on surfaces, *Anal. Chem,* **73,** 1896–1902 (2001).
14. L. Rayleigh, *Proc. R. Soc.* **14** 184–186 (1882).
15. B. Vonnegut and R. L. Neubauer, Production of monodisperse liquid particles by electrical atomization, *J. Colloid Sci,* **7,** 616–622 (1952).
16. G. Taylor, Disintegration of water drops in an electric field, *Proc. Roy. Soc. London, A* **280,** 383–397 (1964).
17. H Kawamoto, Ionic Wind in Pin-to-Plate Corona Discharge System, *Trans. Jpn Soc. Mech. Eng.* **70,** 689, 169–175 (2004).
18. J. N. Smith, R. C. Flagan and J. L. Beauchamp, Droplet evaporation and discharge dynamics in electrospray ionization, *J. Phys. Chem, A* **106,** 9957–9967 (2002).